

Research Papers

Life prediction model for lithium-ion battery via a 3D convolutional network enhanced by channel attention considering charging and discharging process



Zeyu Jiang^a, Tian Peng^{a,b,*}, Zihan Tao^a, Muhammad Shahzad Nazir^a, Chu Zhang^{a,b}

^a Faculty of Automation, Huaiyin Institute of Technology, Huai'an 223003, China

^b Jiangsu Permanent Magnet Motor Engineering Research Center, Huaiyin Institute of Technology, Huai'an 223003, China

ARTICLE INFO

Keywords:

Lithium battery
Battery life prediction
Remaining useful life prediction
Time-series imaging
Depthwise separable convolution

ABSTRACT

While lithium batteries provide high efficiency and low cost, accurately predicting the cycle life of batteries under different charging protocols remains a challenge. The usage of batteries with inadequate cycle life can potentially introduce safety hazards. In this study, a Depthwise Separable 3D Convolutional Network Model Fusing Channel Attention (DS-3DCA-CNN) model considering charging and discharging process is proposed for life prediction of lithium batteries. Firstly, the recurrence plot is used to transform varied cycle charging data into multidimensional form, simultaneously extracting relevant features from discharging data and analyzing their correlation with battery cycle life. Secondly, the Depthwise Separable 3D convolution is used for quicker model training with fewer parameter calculations and introduce a 3D Channel Attention (3DCA) module to increase channel interactions while keeping model complexity low. Finally, ablation experiments are conducted to explore the influence of different time series imaging methods on the accuracy of model prediction results. Experimental results reveal that the proposed DS-3DCA-CNN model, using only 10 initial cycles, predicts battery cycle life with an average error of 35 cycles and achieves a 16-cycle average error when predicting remaining useful life with 20 window cycles of data.

1. Introduction

1.1. Background

Lithium batteries are widely used in many fields due to its long service period and high energy density [1]. However, battery life is generally affected by battery operation and environmental conditions, such as charging rate, voltage, current and temperature during operation [2]. During the service period of the battery, its performance can degrade as the remaining useful life (RUL) of the battery changes [3]. Moreover, even if the lithium battery is produced in the same batch, its final cycle life may not be the same. Using a battery with a sub-standard cycle life can pose a safety hazard because the battery will degrade prematurely. Therefore, a thorough and repeated evaluation of cycle life is necessary during the early testing of the battery to ensure that the battery meets the standard requirements [4]. But as with many tests of complex systems, battery life tests usually take months or even years, which significantly increases the time cost of experiments [5].

To solve this problem, methods of predicting the battery cycle life with external data have been proposed. These methods aim to use the data collected in the early cycles to predict the battery cycle life or RUL, so as to significantly reduce the time required for battery life experiments and provide more opportunities for the production and use of batteries [6]. Therefore, accurately predicting the battery life situation is a key goal for battery fault prediction and shortening the experiment time.

1.2. Literature review

Lithium battery cycle life prediction is traditionally categorized into two types: model-based methods and data-driven methods. Model-based approaches involve the development of various physical or empirical models that describe the degradation process of the battery. These models typically consist of a set of algebraic or differential equations [7]. Zhang et al. [8] proposed a novel model for lithium batteries, called the open circuit voltage and state of charge (OCV-SOC) model, based on

* Corresponding author at: Faculty of Automation, Huaiyin Institute of Technology, Huai'an 223003, China.

E-mail addresses: zeyujiang4-c@my.cityu.edu.hk (Z. Jiang), hushydropt@126.com (T. Peng).

fractional calculus. They compared the root-mean-square error and determination coefficient of their model with a benchmark model under fair conditions. Jia et al. [9] proposed a physics-based model to mitigate the battery aging of electric vehicles (EVs). By formulating a multi-objective optimization function and the state-space equation describing battery aging behavior, the inherent relationships between vehicle speed, acceleration, and SOC of the battery are unveiled. Simulation results indicate that varying degrees of battery life extension can be achieved under a variety of traffic flow conditions. Hooman et al. [10] introduced a new Thévenin-type model for terminal voltage in rechargeable batteries by incorporating nonlinear capacitor elements into the circuit. A key advantage of model-based methods is their lower computational complexity. However, these models fail to consider various influencing factors and are challenging to apply in practical engineering scenarios. With advancements in computing power and machine learning algorithms, data-driven methods have gained popularity for predicting battery cycle life or RUL [11]. In recent studies, data-driven approaches have emerged to address the non-linearity and heterogeneity of lithium-ion battery capacity degradation patterns. Therefore, integrating model-based and data-driven approaches is a promising research direction. For instance, Zhang et al. [12] extracted 6 physical features from voltage relaxation data to indicate battery performance degradation, and then employed data-driven techniques to predict battery life. Experimental results demonstrate that the prediction error of battery life is less than 60 cycles, with a classification accuracy exceeding 90 %.

For those exclusively focused on data-driven methodologies, which can be broadly categorized into two modeling techniques: classification modeling and regression modeling. Classification modeling aims to identify the state of health (SOH) degradation of batteries during the initial stages using classification methods. For instance, Saxena et al. [13] discussed the issue of abnormal capacity decay behavior of battery production batches and proposed two one-class SVM-based methods to detect this behavior in the early stages of battery qualification testing to prevent the transportation of inferior batteries. Another study by Lee et al. [14] identified the inflection point in the charging cycle by measuring the curvature radius of the nonlinear SOH degradation curve. Regression-based modeling aims to forecast the future SOH value or estimate the cycle numbers required for the SOH to reach a specific level using lithium battery data. Severson et al. [15] introduced a cycle life prediction method for early cycles, where they constructed a feature-based linear model using data from the initial 100 cycles. Tao et al. [16] introduced a hybrid deep learning model based on two-dimensional Convolutional Neural Network (CNN2D), Gate Recurrent Unit (GRU), and Improved Manta Ray Foraging Optimization (IMRFO) algorithm for performance degradation prediction of the fuel battery. The experimental results show that the prediction accuracy can reach 79 %. In a different approach, Ji et al. [17] proposed a novel deep learning model that utilizes knee point probability (KPP) to achieve precise degradation prediction for lithium-ion batteries. Additionally, Zhang et al. [18] utilized a moving window-based strategy to model the charging process of the data for predicting battery life and conducting quick classification. This approach leverages Gaussian process regression (GPR) and support vector machine (SVM) for battery life prediction and classification respectively, with experimental results indicating the ability to achieve lower prediction errors in cycle life and knee point.

Most of the state-of-the-art methods mentioned above offer solutions into battery degradation from a singular perspective. Nonetheless, they face constraints due to the multitude of factors influencing battery degradation and the robust interrelations among them. To adequately depict the battery degradation phenomenon, it is imperative to contemplate these factors from various facets throughout the battery's charging and discharging cycles. Wang et al. [19] addressed this issue by organizing battery measurement data from various sensors into a graph structure and leveraging feature fusion based on a graph neural network to enhance network capacity. This approach alleviated the burden of

network design and improved adaptability. Lin et al. [20] proposed an SOH estimation method utilizing a multi-source features long short-term memory (LSTM) network. Zhang et al. [21] took into account the impact of fast charging protocols on battery life and presented a lithium-ion battery life prediction model based on charging and discharging data.

Recent deep learning methodologies demonstrate the ability to handle intricate multi-dimensional datasets, extract effective patterns from datasets and perform feature fusion. Li et al. [22] concatenated continuous data into 3D images and used pruned convolutional neural networks (CNNs) to predict capacity. Experimental results demonstrate the effectiveness of this framework in forecasting battery capacity yet fell short in addressing the significant computational overhead associated with 3D convolutions. Yang et al. [23] employed the auxiliary feature attention mechanism to integrate 3D and 2D CNNs for enhanced predictive performance. While the approach utilized 2D-3D hybrid convolutions to enhance the data interaction between measurements, it overlooked the unsuitability of both 2DCNN and 3DCNN for analyzing one-dimensional time series data. Such convolutional methods could lead to the loss of crucial features and the complex data concatenation might further impede model generalization. By contrast, Lee et al. [24] introduced a CNN architecture that highlights the time-series features of the data by converting capacity degradation data into 2D images. According to their method, a time-series imaging method, namely recurrence plot [25], is used to transform one-dimensional data in the battery charging process into two-dimensional images, so as to highlight the time-series features of the data. Various studies have indicated that employing CNN models with time-series imaging methods yields superior results in classification and regression tasks compared to using raw time-series data [26,27]. Nevertheless, the proposed resolution hinges exclusively on the initial SOH measurements of a battery to predict forthcoming SOH values, potentially leading the model to overfitting and uncovering meaningless patterns within the data.

1.3. Research gap and novelty

The aforementioned studies have yielded favorable outcomes in predicting lithium battery degradation, demonstrating commendable performance on specific datasets. Nonetheless, certain limitations persist:

(1) The majority of current lithium battery life prediction pipelines fail to consider the coupling relationships between various measurement values during the pattern mining component. Measurements from different sensors are merely concatenated, resulting in a decoupling of the statistics when projected into the latent space. Insufficient data interaction hinders the model's ability to extract comprehensive information about global battery degradation.

(2) Lithium batteries harbor latent degradation information during both charging and discharging processes, yet numerous solutions exhibit partiality in addressing battery degradation concerns. Moreover, battery Health Indicators (HIs) based on multi-source features often possess diverse dimensions. While techniques like CNNs can extract patterns from measurements across various dimensions, they still encounter challenges in handling time-series features and lack requisite generalization amidst varied charging protocol scenarios when designing overly intricate models.

To address the above shortcomings and the intricacies associated with network design, a novel approach is proposed in this work. It involves a data dimensionality enhancement technique based on time-series imaging, coupled with a channel attention algorithm to augment interactions between each channel. The key contributions of this study are summarized as follows:

(1) The degradation HIs are derived by analyzing the incremental capacity curve and voltage variation curve during the discharging process of a lithium battery. Furthermore, the HIs and potential patterns of the charging process are integrated via a pipeline based on CNNs structure for multi-feature fusion. In contrast to assessing degradation

characteristics from a singular perspective, this global-based approach enables a more comprehensive description of the battery aging phenomenon.

(2) A time-series imaging methodology is proposed by transforming one-dimensional temporal data into recurrence plots to construct multiple similarity matrices, with the objective of investigating patterns in charging data across various temporal scales. Compared to the direct stacking approach involving charging current, voltage, and temperature data, the proposed solution proves more conducive to extracting profound features from constrained datasets.

(3) The Depthwise Separable 3D Convolutional Neural Network integrated with Channel Attention Component (DS-3DCA-CNN) is proposed to address the issues of excessive weight parameters and lack of coupled computation between measurements in current solutions. This framework has the capability to minimize parameter calculations in the convolution process, while also considering the significant interconnections among measurements to facilitate data interaction in the initial stages of battery degradation.

(4) A fast prediction pipeline considering charging and discharging situations is proposed, with the capable of simultaneously predicting the lithium battery cycle life and remaining useful life under different charging protocols. The proposed approach demonstrates a superior generality compared to the experiments conducted under same charging protocol. The effectiveness of the proposed method is verified by different evaluation metrics and time-series imaging ablation studies.

The rest of this paper is organized as follows. Section 2 describes the scheme for extracting features from the charging and discharging data of lithium batteries and external data. Section 3 proposes the model building method based on multi-dimensional feature fusion. Experimental validation and ablation studies of the proposed method and model are performed in Section 4. The conclusions are given in Section 5.

2. Input data generation and feature analysis

The degradation process of batteries involves intricate thermoelectric coupling, making it challenging to directly measure the battery life situation. Instead, a common approach is to assess the cycle life and RUL by analyzing the voltage, current, and temperature curves obtained during charging and discharging cycles. In contrast to conventional feature-based methods, this section introduces an approach that generates input data from the charging and discharging processes separately. By combining the strengths of machine learning, this method automatically extracts features while also allowing for manual feature selection. This comprehensive approach aims to provide a more detailed description of battery degradation between different cycles.

2.1. Data generation and processing for charging process

2.1.1. Data generation

In the practical application or early development process of lithium batteries, the charging process of the battery is usually relatively gentle and controlled by the charging device. Therefore, it is easy and accurate to measure the external performance of the battery including charging capacity, open circuit voltage, surface temperature and so on. A widely adopted charging strategy, known as CC-CV charging, is based on a commonly used charging protocol that combines constant current (CC) and constant voltage (CV) charging. This approach involves initially applying CC charging until reaching the cutoff voltage, followed by maintaining CV charging until reaching 100 % SOC [28].

The two datasets selected in this paper use 72 and 9 different fast charging protocols, respectively. As far as we know, different charging protocols have different effects on the battery cycle life and RUL. Generally, the lithium battery charging protocol comprises various parameters, including charging rate, charging temperature, cut-off voltage, and charging strategy. Increasing the charging rate can

reduce the charging time; however, it can simultaneously elevate the internal battery temperature, resulting in thermal runaway and chemical imbalance. Additionally, the chosen charging strategy also influences battery health. Employing pulse charging can prolong the battery's cycle life by providing the battery with a "rest period" to mitigate heat build-up.

Although using datasets with various charging protocols adds complexity to the task due to their intricate association with nonlinear degradation processes in batteries, employing different charging protocols also enhances the method's generalization and facilitates its application to other datasets.

The battery cycle life is primarily determined by its internal performance, which manifests through its external electrical and thermal characteristics. To assess battery degradation, the stability of the charging process can serve as an indicator, along with external electrical and thermal properties such as current, voltage, and temperature (VIT) data. However, there is currently no established quantitative formula to precisely describe the relationship between battery life and the charging VIT curve, and no method has been proposed to deal with this common scenario [29]. To address this challenge and leverage the morphological features while ensuring applicability across various charging protocols, VIT data during the battery charging process is adopted as input for the model. The CNN architecture automatically extracts hidden features from the VIT curve to enable accurate analysis.

2.1.2. Data processing with recurrence plots

In this paper, the voltage, current and temperature of battery charging process are treated as a function of capacity ratio, and these data are composed of one-dimensional data of different cycles. Although deep learning methods can directly deal with one-dimensional data, such as 1DCNN and LSTM [30], etc., most of methods fail to capture the spatial relationship between voltage, current and temperature data. In this paper, the stacking of Recurrence Plots is used to map the spatial relationship between data.

Recurrence Plots (RP) is a computational approach that captures the distances between trajectories derived from original time-series data. It serves as a vital method for analyzing periodicity, chaos, and non-stationarity in time-series. By revealing the internal structure of time-series, RP offers valuable insights into similarity, information content, and predictability. Particularly well-suited for short time-series data, RP enables the examination of stationarity and intrinsic similarity within time-series. Its calculation principle is as follows: for the time-series $u_k(k = 1, 2, \dots, n)$ with sample size n and sampling time interval Δt , reconstructing this time-series after embedding dimension m and delay time τ , the reconstructed expression can be obtained as $x_i = (u_i, u_{i+\tau}, \dots, u_{i+(m-1)\tau})$, $i = 1, 2, \dots, n - (m-1)\tau$. Then the distance between points x_i and x_j in the reconstructed space can be expressed as Eq. (1):

$$s_{ij} = \|x_i - x_j\|, i, j = 1, 2, \dots, n - (m-1)\tau \quad (1)$$

Then calculate the recursive value:

$$R(i, j) = H(\epsilon_i - s_{ij}), i, j = 1, 2, \dots, n \quad (2)$$

where ϵ_i is the threshold value, which can be fixed or changed with i , and $H(x)$ represents the Heaviside function [31]. In this paper, to improve the accuracy of the data, the threshold step is skipped, and two-dimensional grayscale images are generated directly.

For the generation of RPs, to reduce computational complexity, this investigation embraces for capacity ratio collection rather than sampling time. Charging capacity is divided into 110 equal partitions (ranging from 0 to 1.1 Ah), with each 0.01 Ah serving as a data sampling point for voltage, current, and temperature. By employing Eq. (1) and Eq. (2) for computing the similarity matrix between each sampling point and its counterparts, a resultant RP matrix measuring 110×110 in both width and height can be procured. For each point in the RP, it represents

the similarity between the sampling point of its abscissa and the sampling point of its ordinate, which is the relative distance. Compared with the original time-series data, the similarity matrix has one more dimension, which can more clearly describe the variability degree between every two sampling points during the charging process of the battery and contains more information. Meanwhile, the calculation of RP is also a process of data normalization, which makes the feature map easier to be extracted by the CNNs.

Fig. 1(a)-(d), (e)-(h), and (i)-(m) depict the transformation of one-dimensional time-series data into two-dimensional RP-VIT matrix in charging process for voltage, current, and temperature cycles of 10, 150, 300, and 450, respectively. To show the variability of data in the similarity matrix more clearly, heat maps are used here. From the figure, it is evident that as the number of batteries charging cycles increases from 10 to 450, the heat maps of voltage, current and temperature change significantly. This phenomenon indicates that the similarity between each sampling point changes with the increase of the cycle period, which also means that the battery degradation information is included. The converted RP-VIT data show accelerated drift in the cycle of 300–450, which is exactly the knee point of the accelerated decay of SOH value, indicating that the knee point of accelerated drift of RP-VIT and accelerated decay of SOH are simultaneously generated. When observing the RP heatmap from 10 cycles to 150 cycles, the degradation of the battery can be seen. This means that although the capacity degradation trends in lithium batteries appear to be similar overall, small differences in battery degradation can still be seen from the transformation RP square

matrix.

In this way, the RP imaging method can also input the cycle number of a battery charging into the model as time-series information and as an input to the third dimension. In fact, the process of time-series transformation is essentially a process of data dimensionality increase, which means that the amount of information increases, such as increasing the representation of the relationship between the data values at different sampling points. Then CNN can obtain more hidden features from it, which means that the model can extract more information about battery degradation in the case of fewer charging and discharging cycles.

Furthermore, the time-series imaging process is also a data normalization process. Throughout the battery charging process, the voltage, current, and temperature data of the battery are recorded in various units. This variation in units can hinder model training and result in lower model accuracy. To eliminate this effect, in the calculation process of RP imaging, VIT data are converted into data with a range distribution of 0–1 to balance the data distribution. RP transformation process is also a data processing process, which highlights the main features of data, and provides a premise for borrowing feature extraction mechanisms from the field of computer vision.

2.2. Feature extraction and analysis for discharging process

In addition to the charging process, the initial discharging cycles of the lithium battery also contain degradation information, therefore, the analysis of discharge component should also be factored in. Although in

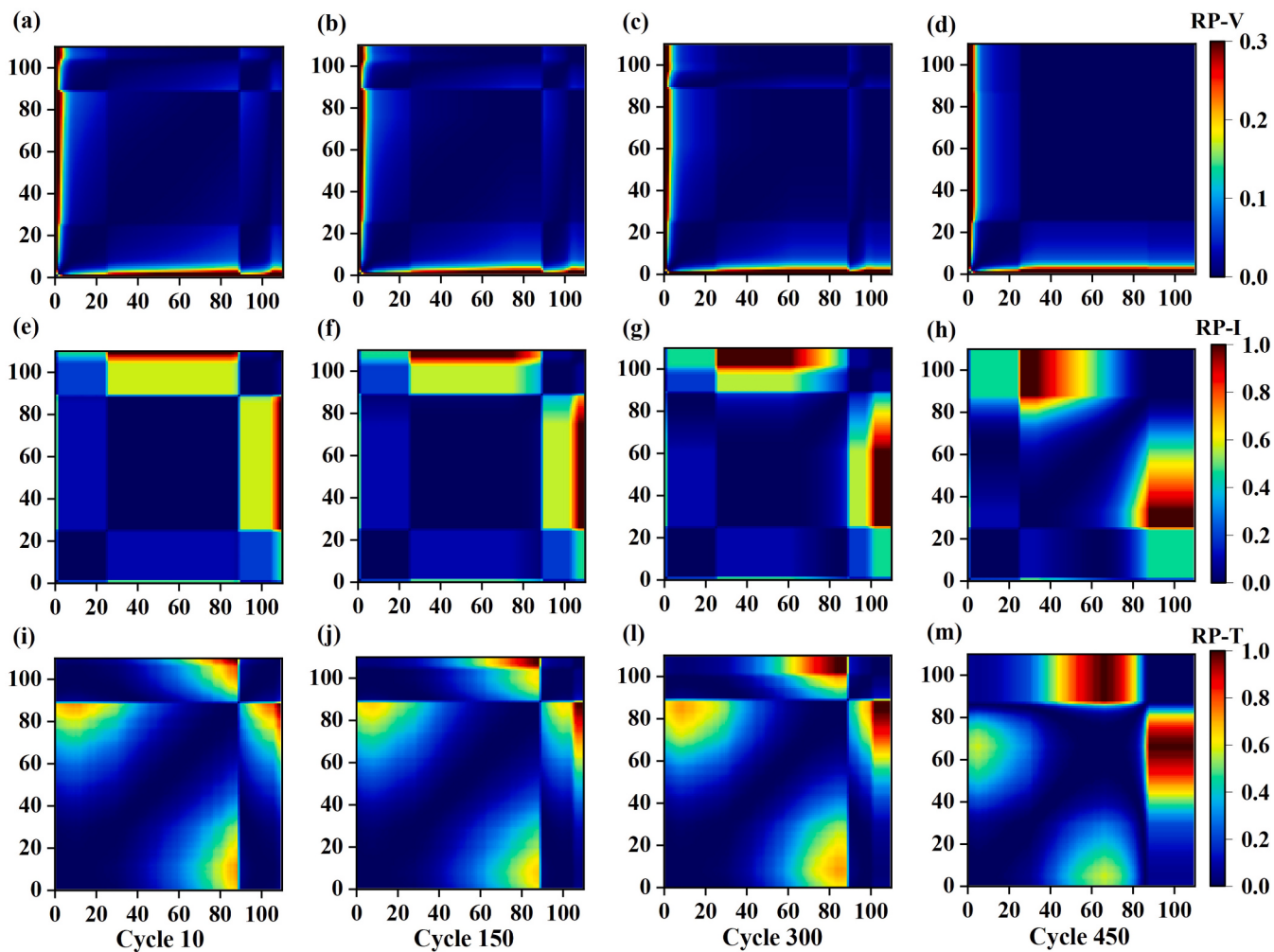


Fig. 1. RP-VIT heatmaps in different cycles: (a) ~ (d) the voltage RP heatmap in 10, 150, 300 and 450 charging cycles; (e) ~ (h) the current RP heatmap in 10, 150, 300 and 450 charging cycles; (i) ~ (m) the temperature RP heatmap in 10, 150, 300 and 450 charging cycles.

practical use, the variability of future profiles loaded on the battery can indeed heighten predictive challenges, typically, the battery discharges under constant current conditions, implying a relatively steadfast discharging current. However, voltage levels and battery surface temperatures may display fluctuations. After the collection and filtration of data, the discharging procedure enables the extraction of HIs from the discharging process via signal processing methods [32]. Due to the uncertainty of battery surface temperature measurement, it is more common to extract features from battery discharge voltage data [33]. For instance, Severson et al. [15] selected 9 features out of 20 to build a prediction model, the feature-based model could predict the cycle life of a battery relying on data from its early cycles. This section will describe how to extract multi-source features from the voltage variation curves of battery discharging process.

2.2.1. Incremental capacity curve analysis

Incremental Capacity (IC) analysis is a method of converting unit voltage changes into easily identifiable peak-valley of electrochemical reaction [34]. The features of the IC curve obtained by this method can indicate the internal electrochemical reaction and reflect the aging process of the battery [35]. The IC can be calculated by the following Eq. (3).

$$IC = \frac{dQ}{dV} = I \frac{dt}{dV} \quad (3)$$

where Q is the battery capacity in the current state, V is the voltage, I is the discharging current, t is the sampling time, and IC represents the voltage of step ratio (dQ/dV). As the voltage step window moves, the complete relationship between incremental capacity and voltage can be obtained.

It can be seen from the transformation of Eq. (3) that IC is negatively correlated with the derivative of voltage with respect to time, indicating that the more gradual the voltage change, the larger the IC value. Fig. 2 illustrates the different feature extraction curves during discharge. As shown in Fig. 2(a) and (b), compared with extracting features directly

from the Q-V curve, the IC curve has more significant features in different discharging cycles of the battery, and the most obvious feature is the drift of the peak of IC curve. It can be seen that as the battery cycle number increases, the peak height decreases and moves sideways to the left. Therefore, the peak coordinates of the IC curve (PICC) are considered as key features of the IC curve. The abscissa is denoted as A1, and the ordinate is denoted as B1.

2.2.2. Discharging voltage curve analysis

In Fig. 2(a), the discharge capacity $Q(V)$ is considered as a function of the voltage in a given cycle, and the features of the discharging voltage are extracted from the curve. Since the voltage range is the same for each cycle, the capacity is considered as a function of voltage to maintain a uniform basis for comparing cycles. As mentioned before, directly extracting features from Q-V curve is not a good method, here the method proposed by Severson et al. [15] is referred. Fig. 2(c) shows the discharging voltage variation curve between cycle i and cycle j , which can be denoted as $\Delta Q_{i-j}(V) = Q_i(V) - Q_j(V)$, where i and j both denote the number of cycles, and the larger the difference between values of i and j is, the more obvious the curve of $\Delta Q_{i-j}(V)$ is. Moreover, it can be seen from the $\Delta Q(V)$ curve that for the same values of i and j , the peak value of the $\Delta Q(V)$ curve (PQVC) of batteries with different cycle lifetimes is different, and the peak value of the battery with longer cycle lifetimes is smaller, indicating that it contains relevant information about battery degradation. Therefore, the value of PQVC can also be selected as a key feature, denoted as B2.

To describe the variation of $\Delta Q(V)$ more intuitively, the Earth Mover's distance (EMD) is introduced in this paper to measure the difference between two adjacent periodic $\Delta Q(V)$ curves. The EMD, also known as Wasserstein distance, is defined as an estimate of the minimum cost of converting from P distribution to Q distribution. Compared with Kullback-Leibler (KL) Divergence [36] and Jensen-Shannon (JS) Divergence [37], EMD can reflect the distance of two distributions even if there is no overlap or the overlap is very small. $W(P, Q)$ denotes the EMD between two probability distributions and can be defined as

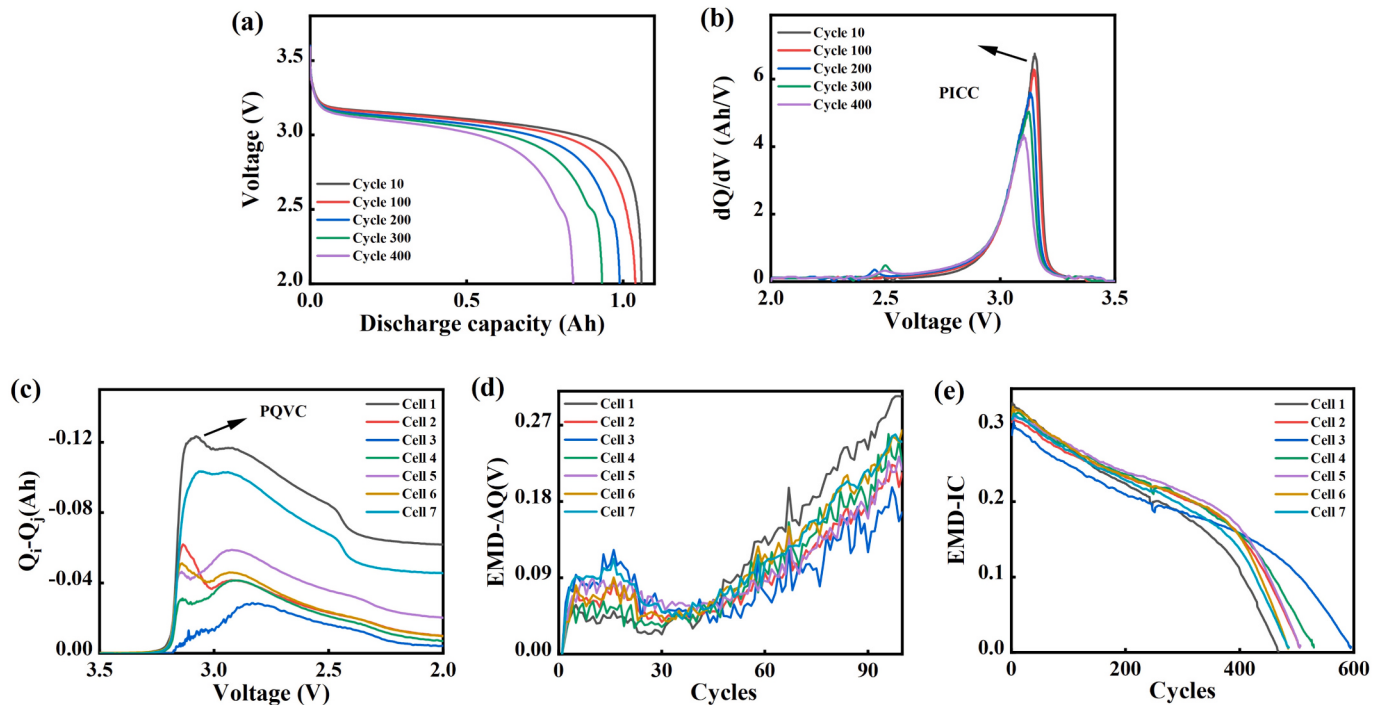


Fig. 2. Feature extraction based on discharging process: (a) Q-V curves of the battery under different cycles; (b) incremental capacity curves of the battery under different cycles; (c) $\Delta Q_{i-j}(V)$ curves of 7 cells based on discharging process; (d) EMD- $\Delta Q(V)$ curves of 7 cells for the first 100 cycles; (e) EMD-IC curves of 7 cells based on the whole cycle life.

follows:

$$W(P, Q) = \inf_{\gamma \in \prod(P, Q)} E_{(x,y) \sim \gamma} [\|x - y\|] \quad (4)$$

where P and Q are the distributions of IC curves of two adjacent cycles, γ is the joint distribution, $\prod(P, Q)$ is the set of all joint distributions of P and Q , and $\|x - y\|$ is the distance between samples. The expectation of the distance $E_{(x,y) \sim \gamma} [\|x - y\|]$ is calculated as follows:

$$E_{(x,y) \sim \gamma} [\|x - y\|] = \sum_i \sum_j P_{(ij)} \|x_i - y_j\| \quad (5)$$

Fig. 2(d) shows the variation trend of EMD- $\Delta Q(V)$ curves between different cells after EMD is introduced to represent the variation of different $i - j$ cycles. As can be seen in the figure, for most cells, the EMD- $\Delta Q(V)$ curve shows an accelerated upward trend within about the first 10 cycles, decreases slightly after reaching the first peak, and continues to increase beyond about 50 cycles (although the chemical and degradation mechanisms are unknown). In addition, the EMD- $\Delta Q(V)$ curve has different trends for batteries with different cycle lifetimes, so it can also be used as the key feature to describe battery degradation [38].

Similarly, we can also generate EMD-IC curves from IC curves. **Fig. 2(e)** shows the EMD variation trend of IC curves between different cells, it can be seen from the figure that the EMD-IC curve gradually decreases as the battery cycle number increases. After 400 cycles, most cells show a decreasing trend in speedup ratio, and there are differences in the decreasing trend of curve for each cell. From the above results, it can be seen that the EMD-IC curve has a certain correlation with battery lifetime, which will be verified in the following sections.

2.2.3. Discharging feature analysis

As mentioned before, two types of input data were generated from the lithium battery charging and discharging process, respectively. Firstly, for the data acquired by the battery during charging, feature analysis is no longer necessary here since it relies on the CNN model to automatically extract hidden features. Secondly, five key features were manually extracted from the voltage data in the battery discharging process. **Table 1** presents the selected features from the discharging process mentioned in this paper. In the feature selection method, these feature curves were selected based on their predictive power rather than their physical meaning.

To validate the adequacy of the selected features in relation to the battery cycle life, it is necessary to perform correlation calculations for each feature mentioned in **Fig. 3**. In the realm of data mining, there are three main proximity measures according to their behavior under variable transformation, namely Cosine Similarity, Correlation, and Euclidean Distance, with different proximity measures being sensitive to different transformations. In this study, the Pearson Correlation is adopted as compared with Euclidean Distance and Cosine Similarity, it is invariant to scaling and translation operations, which is more conducive to uncovering meaningful patterns. Mathematically, for a dataset containing m sets of battery discharging data, the expression for average Pearson Correlation $P_{corr}(x)$ is:

$$P_{corr}(x) = \frac{1}{m} \sum_{k=1}^m \sum_{i=1}^n \frac{(a_i - \bar{a})(b_i - \bar{b})}{\sqrt{(a_i - \bar{a})^2(b_i - \bar{b})^2}} \quad (6)$$

Table 1

Key features extracted from discharging process.

No.	Description
A1	The abscissa of the PICC
B1	The ordinate of the PICC
B2	The ordinate of the PQVC
EMD- $\Delta Q(V)$	Wasserstein distance of $\Delta Q(V)$ curves
EMD-IC	Wasserstein distance of IC curves

where a_i and b_i denote the sampling points of selected features and battery cycle life, \bar{a} and \bar{b} represent the average value of $\sum_{i=1}^n a_i$ and $\sum_{i=1}^n b_i$, respectively. Performing Pearson Correlation calculations on each pair of selected features and battery cycle life yields the coherence coefficient table depicted in **Fig. 3**. It can be observed from the figure that the feature with the least correlation to battery cycle life is EMD-IC, albeit still reaching 0.82. Furthermore, the correlation coefficients between extracted features also all exceed 0.8, indicating a strong interrelation among these features. Hence, the previously selected five essential features can serve as proxies for the original discharging data and be injected into the model.

In summary, there are two types of input data generated, namely VIT data based on charging process and extracted feature data based on discharging process. Adopting this data generation method has the following benefits:

(1) It ensures the generalization of the method. The data source selected is simple, which is the signal processing of external data (battery terminal voltage, current, surface temperature) during battery charging and discharging, so it can be applied to most lithium battery datasets.

(2) The degradation during battery charging and discharging is considered simultaneously. Describing the aging process of the battery from a single perspective may cause the cycle life or RUL prediction process to fall into a local optimum, and the proposed input data generation method can investigate the battery degradation more comprehensively.

(3) Extracting features from discharging process can reduce complexity and computation without affecting the accuracy of the model. Due to the manual extraction of features from battery discharging process, the CNN model no longer needs to extract hidden features from it, which can greatly reduce the burden of model training.

3. Methodology

In this section, the method to predict cycle life and RUL of the battery is introduced in detail. Firstly, the construction of Depthwise Separable 3D Convolutional Network Model Fusing Channel Attention is described step by step. Secondly, the cycle life and RUL prediction method based on charging and discharging features are introduced.

3.1. Depthwise separable 3D convolutional network model Fusing channel attention (DS-3DCA-CNN)

Three-dimensional convolution is widely used in many feature extraction scenarios. This convolution method can capture the sequential features of data in matrix well. Unlike multi-channel images, there is a strong coupling relationship between V, I, and T data during charging. Therefore, it is necessary to fuse these data under different charging cycles to accurately predict battery life. However, while 3DCNN is good at extracting temporal features, neural networks with multiple 3DCNN layers usually have too many parameters, and this problem can lead to difficulties in model training. In this paper, the depthwise separable 3D convolutional model is proposed, and the channel attention mechanism is introduced to greatly reduce the computational cost while obtaining the battery degradation information between different cycles. **Fig. 4** presents the structural diagram of the model.

3.1.1. Depthwise separable 3D convolution

For one charging cycle, after converting the VIT data to RP-VIT data, there are three 110×110 matrices. This matrix form is very similar to a multichannel image, corresponding to a 110-pixel square image, and has three RGB components (hereinafter referred to as a VIT image). When predicting battery cycle life, taking the first n charge cycles as the prediction window, a 4-dimensional $110 \times 110 \times 3 \times n$ matrix can be obtained. For the feature extraction of this 4-dimensional matrix, the

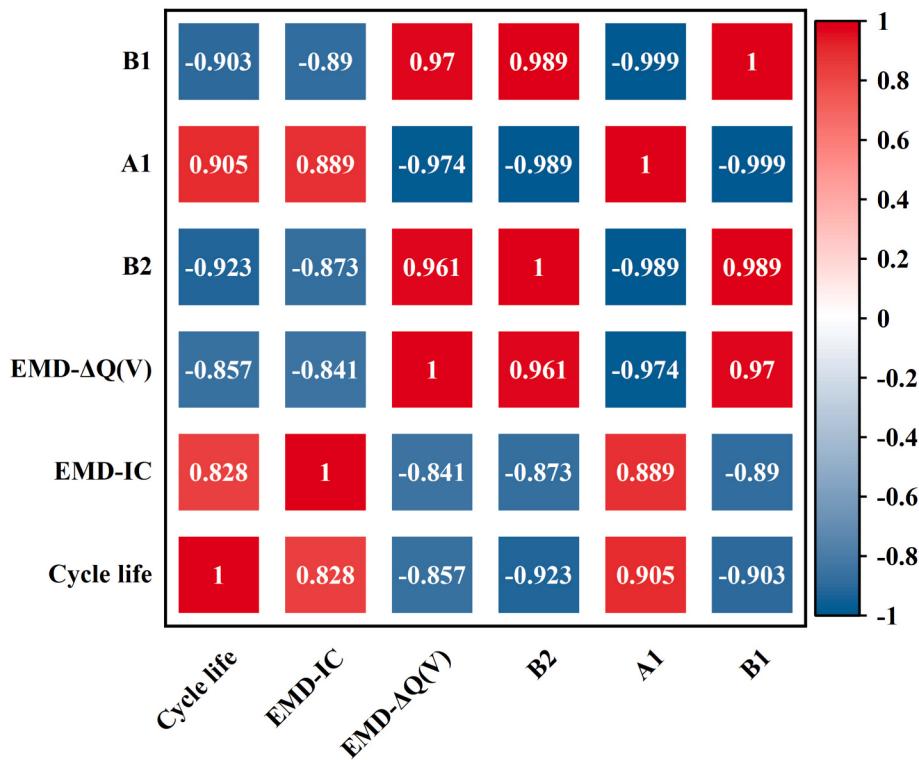


Fig. 3. Pearson correlation coefficient for the five key features and the cycle life.

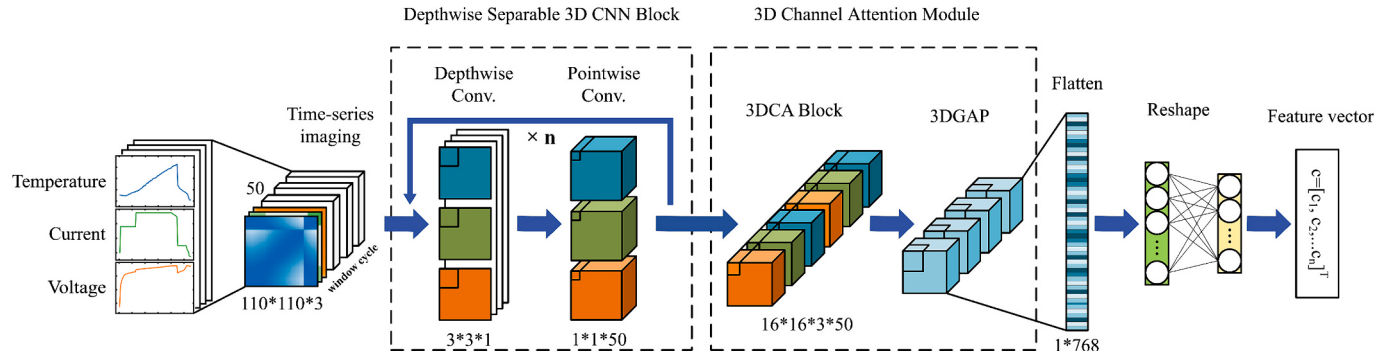


Fig. 4. Structure of proposed DS-3DCA-CNN. Here, the feature vector of lithium battery in the charging process is extracted through several steps: time series imaging, depthwise separable convolution, charging channel attention and perceptron.

common processing method is 3D convolution.

3D convolution is widely used in video classification, point cloud segmentation, 3D medical image feature extraction and other scenarios to extract the temporal features in the data [39]. In this paper, time is replaced by the number of charging cycles as the third dimension. Among them, the calculation formula of 3D convolutional feature map can be expressed by Eq. (6):

$$W_{out} \times H_{out} \times C_{out} \times n = \left(\frac{W_{in} + 2p - w}{s} + 1 \right) \times \left(\frac{H_{in} + 2p - h}{s} + 1 \right) \times \left(\frac{C_{in} + 2p - c}{s} + 1 \right) \times k \quad (7)$$

where $W \times H \times C$ represents the width, height and number of channels of the image, $w \times h \times c$ represents the size of the convolution kernel, s represents the stride, p represents the filling value, k represents the number of scans, and the number of parameters in the convolution process is $(w \times h \times c + 1) \times k$. However, compared with 2DCNN, 3DCNN has one more dimension in calculation, which also leads to more pa-

rameters in the convolution process, and it can impose a large burden on the calculation of the model. Therefore, depthwise separable 3D convolution is used to diminish the difficulty of model training and greatly reduce the amount of convolution calculation.

Depthwise separable convolution [40] is a variant of grouped convolution, where the number of groups corresponds to the channel count of the feature map. Unlike conventional depthwise separable convolution, in this study, the number of channels is replaced by the third dimension of the similarity matrix, representing the cycle number of the battery. As depicted in Fig. 4, for each charging cycle, the similarity matrices of voltage, current, and temperature are concatenated to form a three-dimensional matrix. Compared to standard convolution, this convolution can generate multiple feature maps while the ordinary convolution can only generate one feature map. Nevertheless, since the depthwise convolution layer does not have the information of different cycle periods, a pointwise convolution layer needs to be added.

The pointwise convolution layer is similar to the regular convolution operation, but with kernel size $1 \times 1 \times n$, where n represents the

charging cycles of the first n cycles. The purpose of adding pointwise convolution layer is to perform weighted combination in the depth direction, and the number of feature map can be determined by the number of kernels. Compared with ordinary 3D convolution, in separable 3D convolution block, the matrix only needs to be transformed once, and then the transformed matrix is simply extended to n cycles without transforming the matrix multiple times, which can greatly save computing power. As illustrated in Fig. 4, for a singular Depthwise separable 3D CNN block, perform the 3D convolution in a set of similarity matrix. The kernel size is $3 \times 3 \times 3$ and each operation makes the size of the feature map smaller. This step is similar to the down sampling in conventional 2D U-net, except that it is operated in 3D feature maps. Loop the 3D down sampling until the target feature map size is reached.

To demonstrate the advantages of proposed solution in terms of computational savings, it is crucial to quantify the number of multiplications required during convolution. If the ordinary 3D convolution block with kernel size $3 \times 3 \times 3$ is performed on the similarity matrix of size $110 \times 110 \times 3 \times 50$. This means that there are 3 convolution kernels of size $3 \times 3 \times 3$ moved $108 \times 108 \times 48$ times, which means that the program needs to perform about 45 million multiplication operations. However, for separable convolution, in the first step of depthwise convolution, fifty 3×3 convolution kernels are shifted 108×108 times; in the pointwise convolution, three $1 \times 1 \times 50$ kernels are shifted 108×108 times, which adds up to less than 7 million multiplications. This means that the method proposed in this paper can not only make full use of the advantages of 3D convolution, that is, extract the features between different cycles while obtaining the data features within the same cycle, but also greatly reduce the amount of calculation, so that the network can process more data in a shorter time.

3.1.2. 3D channel attention (3DCA) module

After the depthwise separable 3D convolution operation, the data of V, I, T channels still have not interacted with each other. As described above, there is a strong coupling relationship between voltage, current and temperature during battery charging, so just processing the data like a multi-channel image may not be suitable for the situation in this paper. At the same time, the different features of each channel in the charging process reflect the different states of battery cycle life. To automatically assess the saliency and correlation of various features during the battery charging process for predicting battery life, the 3D Channel Attention (3DCA) module is introduced to learn these features.

The 3DCA module is inspired by the Efficient Channel Attention (ECA) Module proposed by Wang et al., 2020 [41]. In contrast to most attempts at developing more intricate attention modules for improved performance, the ECA module aims to strike a balance between model performance and complexity. It achieves notable performance improvements with minimal additional parameters, demonstrating that suitable cross-channel interaction can effectively reduce model complexity while preserving performance.

Then, based on the ECA Module, the 3DCA module for multi-channel 3D convolution is proposed and applied to the charging process of the battery. Firstly, given the aggregated features $y \in \mathbb{R}^C$ in the charging process, channel attention can be learned by

$$\omega = \sigma(W_k y) \quad (8)$$

where W_k is a parameter matrix of $k \times C$, which can be expressed as:

$$\begin{pmatrix} \omega^{1,1} & \dots & \omega^{1,k} & 0 & 0 & \dots & \dots & 0 \\ 0 & \omega^{2,2} & \dots & \omega^{2,k+1} & 0 & \dots & \dots & 0 \\ \vdots & \vdots & \vdots & \vdots & \ddots & \vdots & \vdots & \vdots \\ 0 & \dots & 0 & 0 & \dots & \omega^{C,C-k+1} & \dots & \omega^{1,1} \end{pmatrix} \quad (9)$$

As for Eq. (8), the weight of y_i is calculated by only considering interaction between y_i and its k neighbors, then the weight can be rewritten as:

$$\omega_i = \sigma\left(\sum_{j=1}^k w_j y_i^j\right), y_i^j \in c_i^k \quad (10)$$

where c_i^k denotes the set of k adjacent channels of y_i , and all channels share the same learning parameters. Note that this method can be easily implemented by a $1 \times 1 \times 1$ convolution kernel with k kernel sizes, i.e.,

$$\omega = \sigma(Convol_k(y)) \quad (11)$$

where $Convol_k$ stands for 3D convolution with kernel size = 1. In addition to this, the degree of interaction between channels can be adjusted by changing the size of k , the kernel size k can be adaptively determined by

$$k = \psi(c) = \left\lceil \frac{\log_2(c) + 1}{2} \right\rceil_{odd} \quad (12)$$

where c represents the number of channels and $\lceil a \rceil_{odd}$ represents the nearest odd distance from a . By mapping ψ , high-dimensional channels have longer range interaction while low-dimensional ones undergo shorter range interaction by using a non-linear mapping.

Fig. 5 shows the structure of the 3DCA layer, where w, h, d represent the width, height and depth of the feature matrix, respectively, and c represents the number of channels of the matrix. Firstly, 3D Global Average Pooling (3DGAP) is calculated on the feature matrix to generate a fully connected layer. After 3D global average pooling, partial channel convolution is performed through k convolution kernels to achieve cross-channel data interaction. Secondly, the number of convolution kernel k is adaptively determined according to the number of channels in the previous layer, and multi-channel convolution is performed to generate channel weights. Finally, the Sigmoid function is used to learn the channel attention. Similar to the ECA module, the proposed method can properly capture local cross-channel interactions while ensuring efficiency and effectiveness, and hardly increasing the parameters for model training.

Finally, a 3DGAP layer is added after the 3DCA layer to reduce the amount of data and computational complexity. According to the correlation between the input data and the battery cycle life, the 3DCA module highlights the specific regions related to cycle life from the feature map and combines the attention layer to detect the saliency of the features of different channels in the input data. As shown in Fig. 4, this module is embedded in the channel attention layer of the DS-3DCNN model after pointwise convolution.

3.2. Model construction combining cycle life and RUL prediction of the battery

The prediction of lithium battery life involves two main processes: charging and discharging. Different charging protocols can have varying effects on battery cycle life. To address this, a machine learning model structure is constructed that combines the feature vectors from both the battery charging and discharging phases. This allows for simultaneous prediction of the battery cycle life and RUL. The term "RUL" refers to the Remaining Useful Life, indicative of the duration for which a battery can effectively operate from its present condition until it becomes unserviceable (often identified when capacity or functionality deteriorates to a pivotal threshold). Ordinarily, RUL, along with SOH and cycle life, exhibits a significant interdependence. SOH plays an imperative role in forecasting RUL as the future usability of a battery is largely contingent upon its current state of health. Meanwhile, Cycle Life serves as a metric reflecting the mean longevity of a battery, deduced from a body of experimental data or statistical analysis. This metric offers insights into the probable lifespan of a battery, and thereby maintains a subtle correlation with RUL. Typically, the SOH tends to diminish as the battery undergoes more discharge and charge cycles, consequently shortening the anticipated RUL.

A visual representation of the prediction process is depicted in Fig. 6.

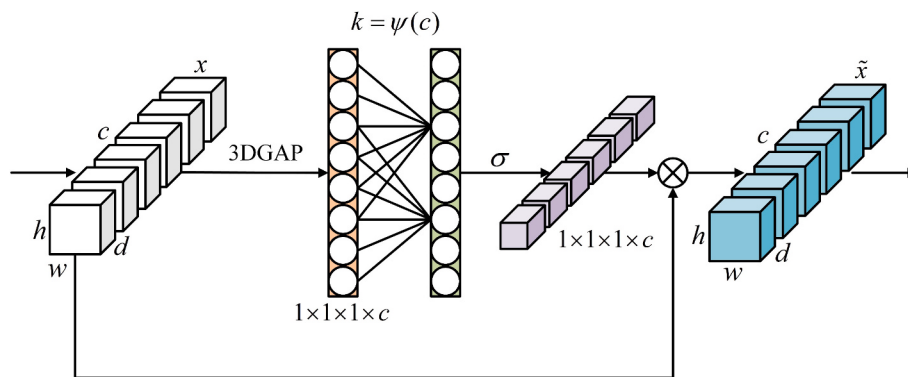


Fig. 5. The structure of 3DCA layer.

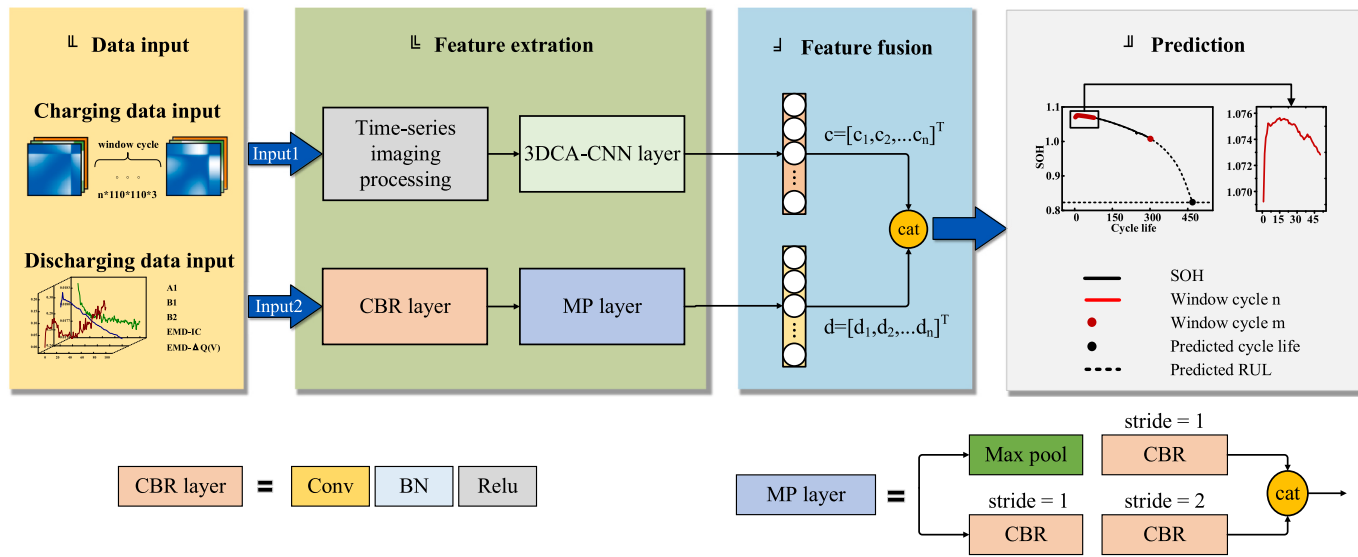


Fig. 6. The flow of lithium battery cycle life and RUL prediction process fusing charging and discharging features.

The process can be divided into four modules: the input module, feature extraction module, feature fusion module, and prediction module. The input module is further divided into two parts: the charging data input part (Input1) and the discharging data input part (Input2), as shown in the figure. The Input1 is responsible for inputting VIT data during the battery charging process and converting the time-series data into RP-VIT data in the next module. The Input2, in turn, is responsible for inputting the features from the battery discharging process manually extracted in Section 2.2.3 into the model.

In addition, the feature extraction module is responsible for extracting hidden features from the data in Input1 and Input2, note that for the extraction of discharging features, the adopted structure is CBR and MP. The CBR structure is constructed by a convolutional layer, a batch Normalization (BN) layer, and a Rectified Linear Unit (Relu) layer. The reason for this structure is that the addition of BN layer can well change the disorder of the original data and accelerate the convergence speed of the network, and have a certain regularization effect, while Relu layer can transform linear transformation into nonlinear transformation. This typical structure has been confirmed in a large number of papers and is a very effective structure [42]. The MP structure mainly consists of a max-pooling layer and several convolutional layers with different stride sizes. The max-pooling layer and the convolutional layer with stride = 2 halve the number of channels and then keep the number of input and output channels constant after concatenation. This structure is also utilized in popular deep learning models, such as the Yolo architecture [43]. It offers the benefit of preserving essential

information by avoiding excessive loss during the pooling layer. Additionally, it allows for feature compression to a certain degree, simplifying network complexity and reducing computational requirements.

Furthermore, the feature fusion module is responsible for fusing the feature vectors from the two sources. After feature extraction, the model faces challenges in learning an effective input-to-output mapping due to the varying dimensions and sizes of these features. Hence, to enhance the model's accuracy, it becomes vital to fuse features of different dimensions. This fusion ensures that the model can acquire comprehensive battery degradation information from diverse feature types. The module converts the features of different dimensions into a one-dimensional feature vector through fully connected layers, which is concatenated together to form a new feature matrix.

Finally, the prediction module is responsible for predicting the battery cycle life and RUL. In this module, the window cycle of the battery is split into the first \$n_f\$ charging cycles and the latest \$m_l\$ charging cycles, and divided into two parts, so as to predict cycle life and RUL of the battery at the same time. The function of the window cycle lies in providing a scope within which observed data can be utilized by models to forecast the cycle life and RUL of lithium batteries. This snapshot of data is commonly employed as the training dataset for model input, equipping the predictive algorithms with relevant historical information to extrapolate future performance metrics. It can be seen from the figure that the battery cycle life prediction only needs the data of \$n_f\$ cycles as input, and the cycle number when the battery SOH drops to a certain

level is used as the output to predict the cycle life of the battery. However, the prediction of RUL requires $n_f + m_l$ cycles of data as input to calculate the mapping relationship with the battery RUL.

4. Experimental verification and analysis

4.1. Experiment introduction and evaluation metrics

In this study, two datasets of LFP/graphite lithium batteries obtained from MIT are utilized as raw data input to validate the proposed prediction method. The batteries used are A123 system's model APR 18650 M1A with a nominal capacity of 1.1 Ah and a nominal voltage of 3.3 V [15]. The datasets were generated by cycling these LFP/graphite cells using a 48-channel Arbin LBT potentiostat, under a controlled temperature of 30 °C. These datasets include the charging process of the battery under various states, with an average current rate ranging from 3.6C to 6C. As a result, they serve as suitable test scenarios for evaluating the capability of the proposed method to predict the battery cycle life and RUL under diverse charging strategies.

After removing part of the problem batteries during data collection, the first dataset with 140 batteries is divided into training set, validation set and test set according to the ratio of about 80 %, 10 % and 10 %. For the second dataset, due to the small sample size, a total of 45 batteries are divided according to the ratio of about 60 %, about 20 % and about 20 % to verify the effectiveness of the method and the proposed model. However, in these two datasets, the cycle life of batteries is unevenly distributed, which ranges from about 140 to 2240, so the model may be biased during training. For instance, during model training, too much data with a battery cycle life interval of 800 to 1000 is input, resulting in excessive deviation in the battery cycle life prediction of 400 to 600 during model testing. This situation reduces the accuracy of the model and affects its generalization ability.

Therefore, to ensure that the model can learn the features of batteries with different cycle life on average, the two datasets are divided into multiple intervals according to the number of cycles, and the training data, validation data and test data of each interval are divided proportionally. Fig. 7 show the results of dataset 1 and dataset 2 divided by cycle life interval respectively. It can be seen that for dataset 1, most cycle lifetimes are concentrated between 400 and 1200, while for dataset 2, there are more cycle lifetimes between 600 and 1000. Finally, the sets of each cycle life interval were merged into the total training set, the total validation set and the total test set. This method can effectively avoid the bias of the model learning caused by the uneven distribution of the dataset.

The experiment is repeated 5 times under the same experimental settings for two data sets, a total of 10 experiments are performed, named Case_0, Case_2, ..., Case_9, but the dataset partition for each

experiment is random. To evaluate the estimation accuracy, mean square error (MSE), mean square log error (MSLE) and mean absolute error (MAE) are used as evaluation indicators, which are calculated as follows:

$$\text{MSE} = \frac{1}{n} \sum_{i=1}^n (\hat{y}_i - y_i)^2 \quad (13)$$

$$\text{MSLE} = \frac{1}{n} \sum_{i=1}^n (\log(\hat{y}_i) - \log(y_i))^2 \quad (14)$$

$$\text{MAE} = \frac{1}{n} \sum_{i=1}^n |\hat{y}_i - y_i| \quad (15)$$

where Eq. (12), Eq. (14), and Eq. (15), n represents the number of batteries, y_i represents the true value, and \hat{y}_i represents the predicted value. MSE is the mean square error, and outliers are given more weight when the error is squared. MSLE is an improvement on MSE, if the range of values to be predicted is widely distributed, MSE will be affected by some large values, and the prediction accuracy for small values will also be reduced. The distribution of battery cycle life in MIT dataset is between 140 and 2240, but most of the datasets are concentrated between 600 and 1200, and only a small number of battery cycle life is greater than 1600, MSLE may be more reasonable for such a wide range of data distribution. MAE is the average of the absolute deviations between predicted values and actual measurements. It provides an accurate reflection of the prediction error. A value closer to 0 for the MAE indicates a higher level of accuracy for the model across these evaluation metrics.

4.2. Results of different window cycles

In this section, to verify the effectiveness of the early prediction of the proposed model, a combination of different sizes of n_f and m_l are selected as the window cycle to test the model performance after completing the model training. Note that n_f represents the first n charging and discharging cycles of the battery, and m_l represents the most recent m cycles.

4.2.1. Results of cycle life prediction for lithium battery

The choice of different window cycle can change the model input data size, which may eventually affect the prediction accuracy of the model. In this paper, different first n charging and discharging cycles ($n_f=10$, $n_f=30$, $n_f=50$) are selected for comparative experiments. Since the input data has been normalized before being fed into the model training, it is necessary to perform the de-normalization calculation first

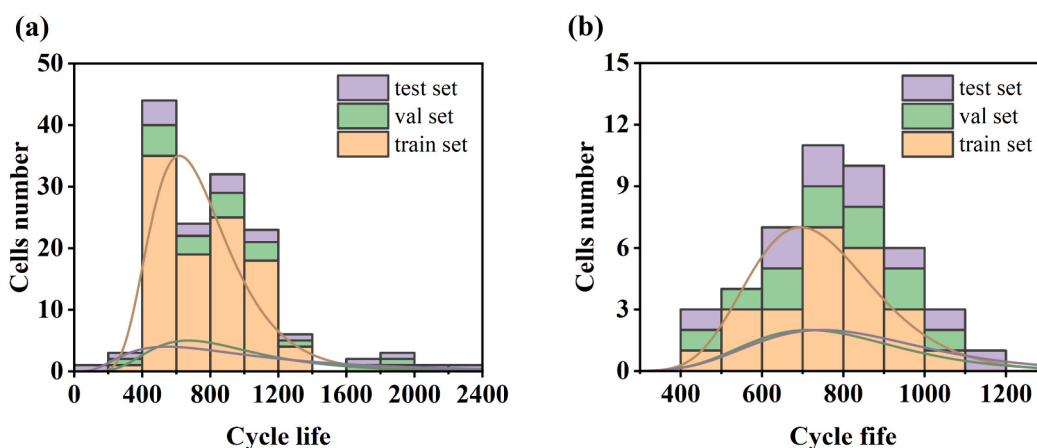


Fig. 7. Distribution and partition of cycle life data.

when performing the prediction result calculation. **Table 2** and **Table 3** show the experimental results of two datasets under different window cycles, and **Fig. 8** show the MAE, MSE, and MSLE results of a total of 10 experiments in the form of line charts.

It is obvious that the error of the model is the smallest when $n_f=50$ compared to the cases $n_f=10$ and $n_f=30$, which means that the battery cycle life can be more accurately predicted when the window cycle is larger. However, when the window cycle is increased from 30 to 50, the reduction of model error is not as large as when the window cycle is increased from 10 to 30.

Table 4 shows the comparison of the results of the proposed model with several other mainstream machine learning models and deep learning models under different window cycle. It can be seen that most models need more than 100 charging and discharging cycles to achieve comparable results with DS-3DCA-CNN. Compared with other models, the proposed model can predict cycle life accurately with fewer window cycle. This result shows that although converting the battery charging VIT data into RP-VIT will increase the data dimension and the amount of calculation, more hidden features can be extracted from the original data through 3D depthwise separable convolution. In particular, when window cycle $n_f = 10$, the average prediction error of the model is only 35 cycles, which is much better than other common models, because it achieves similar results with less data, so it is particularly suitable for battery life prediction with low cycles.

Fig. 9 shows the early battery cycle life prediction results of the proposed model in a total of 10 experimental test sets of two data sets, arranged from small to large according to the actual cycle life, where the window cycle $n_f=10$. The number of batteries in the dataset1 test set is 16, so there are 80 cycle life prediction results after 5 experiments. The battery number in the test set of dataset2 is 9, and a total of 45 prediction results can be obtained after 5 experiments. In the figure, the proposed model is accurate in most cases for the battery life prediction with a cycle life less than 1000, but it is not as good as the former for those with a cycle life larger than 1500. This is caused by the uneven distribution of the MIT dataset in the battery cycle life, only a few batteries have more than 1500 cycles, which makes it difficult for the model to extract more features of high-cycle life batteries during the training process. However, this situation will not have a great impact on the experimental results, because the purpose of cycle life prediction is to predict the possible cycle life in advance through the data of the early battery charging and discharging cycle, so as to judge whether the battery is qualified. For a battery whose cycle life prediction is far from standard, it is not necessary to care whether it can be charged and discharged 2000 or more times.

Fig. 10 presents the boxplots of the error bounds, based on MSLE, $n_f = 10$, for the 10 experimental cases. For most of the experimental cases, the gap between the predicted value and the real value of the

Table 2
Experimental results of dataset1.

Experiment	Metrics	Window cycle		
		10	30	50
case_0	MAE	130	88	61
	MSE	41	31	18
	MSLE	34	22	16
case_1	MAE	125	55	45
	MSE	36	18	12
	MSLE	26	17	14
case_2	MAE	130	93	48
	MSE	58	36	20
	MSLE	25	22	13
case_3	MAE	109	63	43
	MSE	41	24	15
	MSLE	31	13	9
case_4	MAE	114	76	45
	MSE	44	23	14
	MSLE	24	21	12

Table 3
Experimental results of dataset2.

Experiment	Metrics	Window cycle		
		10	30	50
case_5	MAE	117	83	49
	MSE	53	29	15
	MSLE	26	20	20
case_6	MAE	153	129	81
	MSE	90	44	29
	MSLE	60	30	16
case_7	MAE	123	84	61
	MSE	46	29	25
	MSLE	44	21	15
case_8	MAE	132	109	65
	MSE	65	40	20
	MSLE	46	36	22
case_9	MAE	149	91	49
	MSE	55	36	18
	MSLE	36	29	15

battery life is between 20 cycles and 50 cycles, which indicates that the proposed model and method can well capture the degradation information of the battery during training and make an accurate prediction of the cycle life with only a few window cycles.

4.2.2. RUL prediction for lithium battery

Compared with the lithium battery cycle life prediction, its RUL prediction is relatively complicated. In addition to the first n charging and discharging cycles of the battery n_f , it also needs the data of the last few cycles of the battery, denoted m_l . Since there are too many combinations between n_f and m_l , $m_l=3$, $m_l=5$ and $m_l=10$ are chosen as the window cycle for RUL prediction when $n_f=10$ is considered. **Table 5** and **Fig. 11** presents the RUL prediction results for dataset1 and dataset2. As can be seen from the table, similar to the battery cycle life prediction results, the larger the window cycle m_l , the smaller the prediction error.

Fig. 12 shows the comparison between the real RUL and predicted RUL of the batteries of the two datasets when $n_f=10$ and $m_l=3$, where dataset1 contains 16 batteries in the test set and dataset2 contains 9 batteries in the test set. Note that this experiment is performed as a RUL prediction point every 10 cycles. As can be seen from the figure that for different batteries with different charging strategies, their cycle life also varies greatly from about 300–1900 cycles, indicating that different charging strategies have a great impact on the battery cycle life. In the figure, by observing the trend of the curve change, it can be seen that in the initial stage of RUL prediction, that is, when the remaining useful life of the battery is the maximum value, its actual RUL and the predicted RUL results have a large difference. However, as the number of cycles increases, that is, when the RUL of the battery is closer to 0, the predicted RUL result is closer to the true value.

4.3. Ablation study on time-series imaging method

As described in **Section 2**, the 1D VIT data were converted to RP-VIT data by time-series imaging method. This approach increased the data dimension and thus extracted the degradation information during battery charging. To verify the effectiveness of the introduced method, the ablation study [44] is required. Note that in addition to Recurrence Plots, there are other time-series imaging methods such as the Gram Angle Field (GAF) [45] and the Markov Transition Field (MTF) [46], where the GAF is further divided into Gram Angle Sum Field (GASF) and Gram Angle difference Field (GADF). These imaging methods are added together as a control group for the ablation study.

In the testing stage, three metrics are calculated to estimate the model accuracy. For dataset 1 and dataset 2, the results of the two experiments are shown in **Table 6**, and **Fig. 13** shows the radar plot of the error results in both datasets (window cycle $n_f = 10$).

As can be seen from the figure that after transforming the original

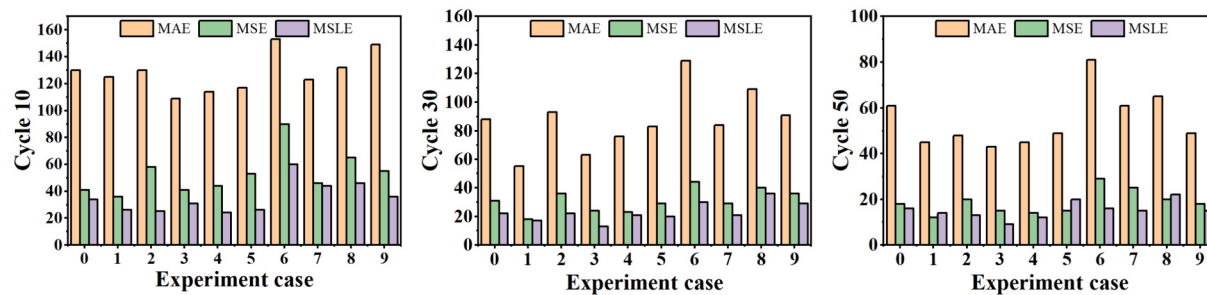


Fig. 8. MAE, MSE and MSLE of experimental results on two datasets.

Table 4
Comparison of different battery cycle life prediction methods.

Model	Window cycle	Metrics		
		MAE	MSE	MSLE
CNN-LSTM	150	116	111	82
ELM	150	98	109	119
TCN	100	93	68	36
Transformer	50	141	71	69
LS-SVM	50	116	54	38
Proposed	50	55	19	15
Proposed	30	87	31	23
Proposed	10	119	52	35

data into RP, GASF, GADF and MTF, their comprehensive error calculation results are close, while directly using the original data does not work as well. The Recurrence Plot reflects the image of the distance between the trajectories extracted from the original time-series, which can reflect the distance change between any two sampling points at different times during the charging process of the VIT data. GAF reflects the transformation between the Angle and/difference between different points in polar coordinates when the original time-series is transformed. MTF grids the data matrix and then replaces the subplots in each grid with the mean. The similarity of these methods is that they all can represent the change between any two sampling points.

Therefore, the results in Fig. 13 first show that the accuracy of the model can be improved by using the time-series imaging method compared to the original one-dimensional data, because more information is generated in the process of increasing the dimensionality of the data. Secondly, the similar results of RP, GAF and MTF indicate that CNN is not sensitive to how the data is calculated, and it only cares about whether there is more effective information in the transformed data.

5. Conclusions

This paper proposed a method to predict battery cycle life and RUL through the early charging and discharging cycles. In this paper, the RP was used as a time-series imaging method to convert the charging data between different charging cycles into a multidimensional image, so as to obtain more complete information about the degradation of lithium batteries. At the same time, effective features were extracted from the

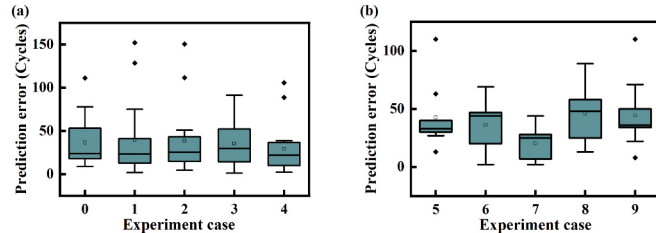


Fig. 10. Boxplots of the error bounds.

Table 5
RUL prediction results for dataset1 and dataset2.

Model	Metrics	Window cycle		
		$m_l=3$	$m_l=5$	$m_l=10$
Dataset1	MAE	59	54	45
	MSE	33	29	16
	MSLE	25	20	13
Dataset2	MAE	64	56	42
	MSE	41	36	33
	MSLE	35	28	18

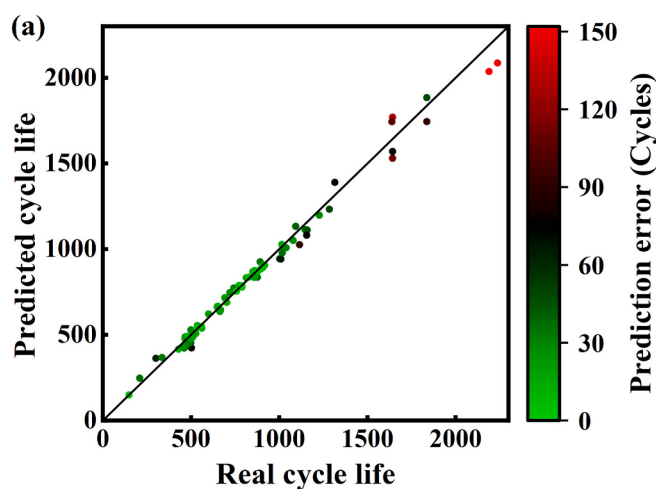


Fig. 9. Results of early cycle life prediction of lithium battery: (a) Results for Dataset1; (b) Results for Dataset2.

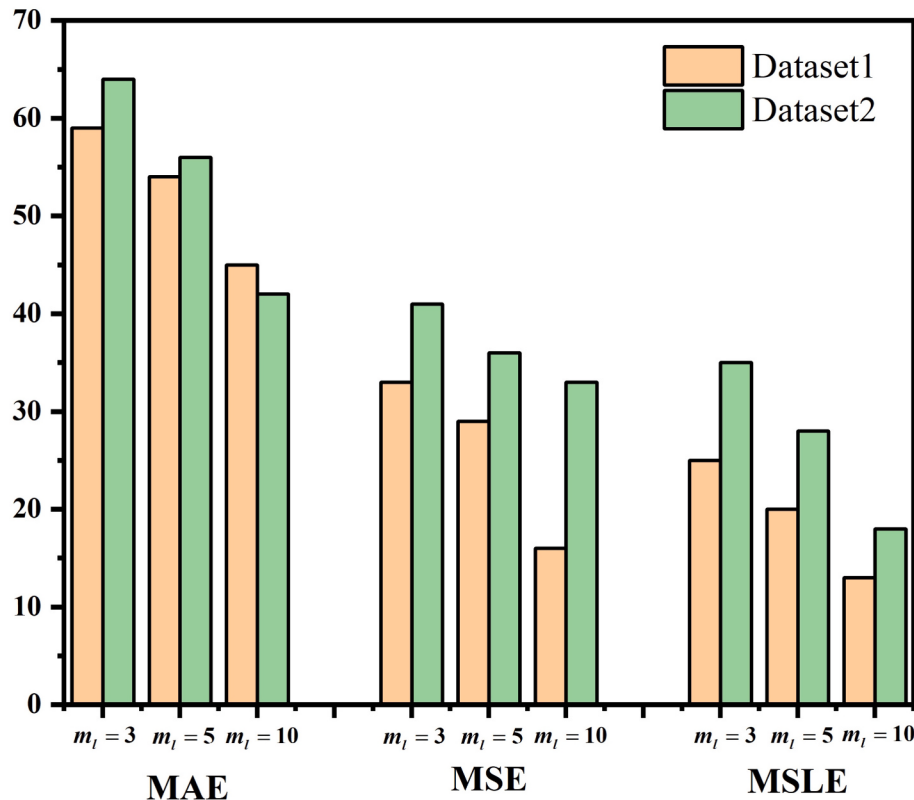


Fig. 11. RUL prediction results for dataset1 and dataset2.

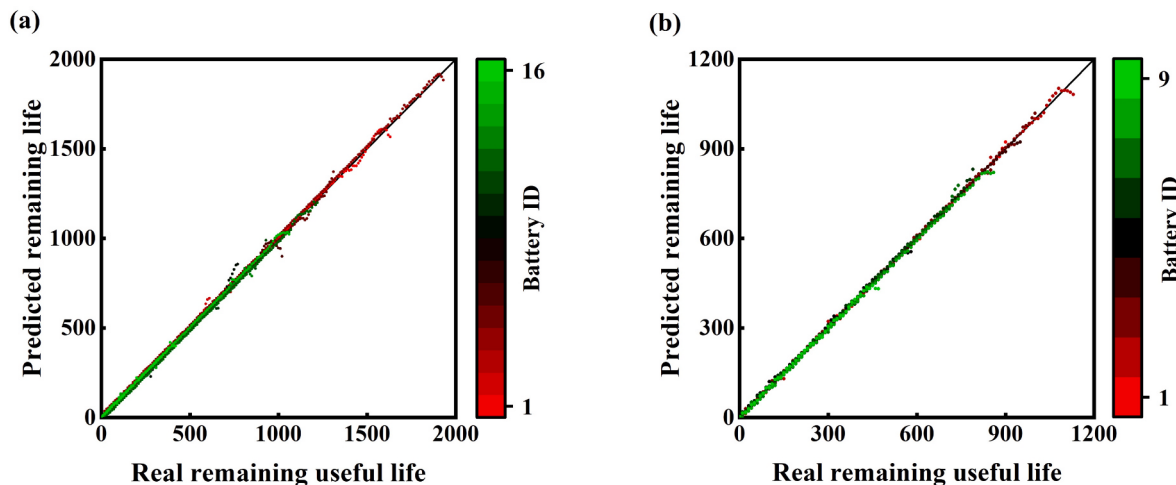


Fig. 12. Results of RUL prediction of lithium battery: (a) Results for Dataset1; (b) Results for Dataset2.

Table 6
Comparison of experimental results of different time-series imaging methods.

Experiment	Metrics	RP	GASF	GADF	MTF	original
Dataset 1	MAE	130	125	106	142	131
	MSE	46	36	49	67	84
	MSLE	32	55	38	46	68
Dataset 2	MAE	105	113	122	136	161
	MSE	46	56	75	57	117
	MSLE	39	44	41	49	71

lithium battery of discharging data, and their correlation with the battery cycle life was analyzed. To speed up the model training and enhance the data interaction between different measurements, the DS-3DCA-CNN model was proposed to process the multi-channel 3D data. During battery charging, the analysis results showed that the proposed model has higher model accuracy and faster model training speed, especially in the face of fewer window cycles, due to the increased data dimension, the amount of information of the original data increased, so it had more advantages than other models. The experimental results showed that the average cycle life prediction error of the proposed model was only 35 cycles even if only the first 10 charging and discharging cycles were used, and when the window cycle increased, the model prediction accuracy further decreased. Finally, the proposed

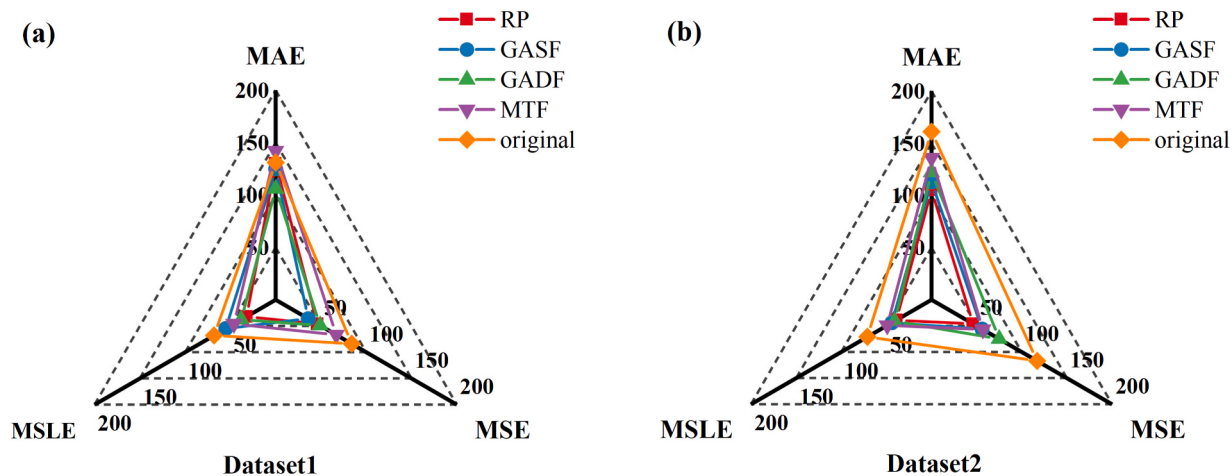


Fig. 13. Radar plot of the error results in both datasets.

model can also predict the RUL of the battery during its use, and thus distinguish the healthy battery from the unhealthy battery in advance.

6. Further research

This paper demonstrates a method that concurrently extracts the charging and discharging characteristics, exhibiting commendable precision and generalization across various fast charging scenarios. Nonetheless, there are still some limiting factors at present:

(1) In this paper, the feature extraction of charging data is primarily carried out through the utilization of image processing pipelines. While this approach yields a satisfactory preservation of characteristics, challenges such as heavy computational burden and complexity in the predicting procedure persist.

(2) It is noted that the experiments were conducted in an ideal setting, unaffected by external factors such as temperature and vibration; moreover, this study operates fast charging and discharging experiments in small-scale lithium batteries, thus the effectiveness for larger batteries remains to be explored.

(3) In the fact that in a certain real-world battery application such as EVs, relying solely on data-driven approaches would exacerbate the challenge of accurately predicting cycle life.

As a result, future research directions include further integrating model-based and data-driven strategies for predicting the cycle life of lithium batteries. In practical applications, the variability of future profiles loaded on the battery may increase prediction challenges, while physical models may offer compensatory solutions, which will be an intriguing research direction.

CRediT authorship contribution statement

Zeyu Jiang: Writing – original draft, Software, Methodology. **Tian Peng:** Writing – review & editing, Visualization. **Zihan Tao:** Writing – review & editing, Data curation. **Muhammad Shahzad Nazir:** Supervision. **Chu Zhang:** Writing – review & editing, Supervision, Software, Conceptualization.

Declaration of competing interest

The authors declare that they have no known competing financial interests or personal relationships that could have appeared to influence the work reported in this study.

Data availability

Data will be made available on request. Data can be accessed through

<https://data.matr.io/1/projects/5d80e633f405260001c0b60a>.

Acknowledgements

This work is supported by the National Natural Science Foundation of China (NSFC) (No. 62303191), the National Natural Science Foundation of China (No. 62306123), the Natural Science Foundation of the Jiangsu Higher Education Institutions of China (No. 23KJD480001), the Double-innovation Doctor Program of Jiangsu province (No. JSSCBS20201033 and No. JSSCBS20201037). Special thanks are given to the Huai'an Innovative Talents Project.

References

- [1] W. He, Z. Li, T. Liu, Z. Liu, X. Guo, J. Du, et al., Research progress and application of deep learning in remaining useful life, state of health and battery thermal management of lithium batteries, *J. Energy Storage* 70 (2023) 107868.
- [2] W. Zhao, W. Ding, S. Zhang, Z. Zhang, A deep learning approach incorporating attention mechanism and transfer learning for lithium-ion battery lifespan prediction, *J. Energy Storage* 75 (2024) 109647.
- [3] L. Xie, F. Ustolin, M.A. Lundteigen, T. Li, Y. Liu, Performance analysis of safety barriers against cascading failures in a battery pack, *Reliab. Eng. Syst. Saf.* 228 (2022) 108804.
- [4] Y. Liu, G. Sun, X. Liu, Remaining useful life prediction of lithium-ion batteries based on peak interval features and deep learning, *J. Energy Storage* 73 (2023) 109308.
- [5] S. Sun, H. Zhang, J. Ge, L. Che, State-of-health estimation for lithium-ion battery using model-based feature optimization and deep extreme learning machine, *J. Energy Storage* 72 (2023) 108732.
- [6] X. Shu, J. Shen, Z. Chen, Y. Zhang, Y. Liu, Y. Lin, Remaining capacity estimation for lithium-ion batteries via co-operation of multi-machine learning algorithms, *Reliab. Eng. Syst. Saf.* 228 (2022) 108821.
- [7] Y. Li, Z. Wei, B. Xiong, D.M. Vilathgamuwa, Adaptive ensemble-based electrochemical-thermal degradation state estimation of lithium-ion batteries, *IEEE Trans. Ind. Electron.* 69 (7) (2022) 6984–6996.
- [8] Q. Zhang, N. Cui, Y. Li, B. Duan, C. Zhang, Fractional calculus based modeling of open circuit voltage of lithium-ion batteries for electric vehicles, *J. Energy Storage* 27 (2020) 100945.
- [9] Y. Jia, G. Luo, Y. Zhang, Development of optimal speed trajectory control strategy for electric vehicles to suppress battery aging, *Green Energy and Intelligent Transportation* 1 (2) (2022) 100030.
- [10] H. Fatourechi, M. Ehrhardt, Numerical and semi-numerical solutions of a modified Thévenin model for calculating terminal voltage of battery cells, *J. Energy Storage* 45 (2022) 103746.
- [11] R. Xiong, J. Tian, W. Shen, J. Lu, F. Sun, Semi-supervised estimation of capacity degradation for lithium ion batteries with electrochemical impedance spectroscopy, *Journal of Energy Chemistry* 76 (2023) 404–413.
- [12] Y. Zhang, X. Feng, M. Zhao, R. Xiong, In-situ battery life prognostics amid mixed operation conditions using physics-driven machine learning, *J. Power Sources* 577 (2023) 233246.
- [13] Saxena S, Kang M, Xing Y, Pecht M. Anomaly Detection During Lithium-ion Battery Qualification Testing. Conference Anomaly Detection During Lithium-ion Battery Qualification Testing. p. 1–6.
- [14] J. Lee, D. Kwon, Pecht MGJIToIE, Reduction of Li-ion battery qualification time based on prognostics and health management 66 (99) (2018) 7310–7315.

- [15] K.A. Severson, P.M. Attia, N. Jin, N. Perkins, B. Jiang, Z. Yang, et al., Data-driven prediction of battery cycle life before capacity degradation, *Nat. Energy* 4 (5) (2019) 383–391.
- [16] Z. Tao, C. Zhang, J. Xiong, H. Hu, J. Ji, T. Peng, et al., Evolutionary gate recurrent unit coupling convolutional neural network and improved manta ray foraging optimization algorithm for performance degradation prediction of PEMFC, *Appl. Energy* 336 (2023) 120821.
- [17] S. Ji, J. Zhu, Z. Lyu, H. You, Y. Zhou, L. Gu, et al., Deep learning enhanced lithium-ion battery nonlinear fading prognosis, *J. Energy Chem.* 78 (2023) 565–573.
- [18] Y. Zhang, M. Zhao, R. Xiong, Online data-driven battery life prediction and quick classification based on partial charging data within 10 min, *J. Power Sources* 594 (2024) 234007.
- [19] Z. Wang, F. Yang, Q. Xu, Y. Wang, H. Yan, M. Xie, Capacity estimation of lithium-ion batteries based on data aggregation and feature fusion via graph neural network, *Appl. Energy* 336 (2023) 120808.
- [20] M. Lin, J. Wu, J. Meng, W. Wang, J. Wu, State of health estimation with attentional long short-term memory network for lithium-ion batteries, *Energy* 268 (2023) 126706.
- [21] C. Zhang, H. Wang, L. Wu, Life prediction model for lithium-ion battery considering fast-charging protocol, *Energy* 263 (2023) 126109.
- [22] Y. Li, K. Li, X. Liu, Y. Wang, L. Zhang, Lithium-ion battery capacity estimation — a pruned convolutional neural network approach assisted with transfer learning, *Appl. Energy* 285 (2021) 116410.
- [23] Y. Yang, A machine-learning prediction method of lithium-ion battery life based on charge process for different applications, *Appl. Energy* 292 (2021) 116897.
- [24] G. Lee, D. Kwon, C. Lee, A convolutional neural network model for SOH estimation of Li-ion batteries with physical interpretability, *Mech. Syst. Signal Process.* 188 (2023) 110004.
- [25] J.P. Eckmann, S.O. Kamphorst, D.J.E.L. Ruelle, Recurrence plots of dynamical systems 4 (9) (1987) 973–977.
- [26] Z. Wang, T.J.A.P. Oates, Imaging Time-Series to Improve Classification and Imputation, 2015.
- [27] H. Zheng, Z. Hu, X. Wang, J. Ni, M. Cui, VMD-CAT: a hybrid model for short-term wind power prediction, *Energy Rep.* 9 (2023) 199–211.
- [28] W. Xie, X. Liu, R. He, Y. Li, X. Gao, X. Li, et al., Challenges and opportunities toward fast-charging of lithium-ion batteries, *J. Energy Storage* 32 (2020) 101837.
- [29] H. Ruan, Z. Wei, W. Shang, X. Wang, H. He, Artificial intelligence-based health diagnostic of Lithium-ion battery leveraging transient stage of constant current and constant voltage charging, *Appl. Energy* 336 (2023) 120751.
- [30] S. Hochreiter, J.J.N.C. Schmidhuber, Long short-term memory 9 (8) (1997) 1735–1780.
- [31] Y. Lu, J. Xu, Li YJJMS, Application of recurrence plot and approximate entropy on complexity analysis of machinery fault signal 59 (4) (2006) 213–216.
- [32] D. Zhou, B. Wang, C. Zhu, F. Zhou, H. Wu, A light-weight feature extractor for lithium-ion battery health prognosis, *Reliab. Eng. Syst. Saf.* 237 (2023) 109352.
- [33] F. Li, Y. Min, Y. Zhang, Y. Zhang, H. Zuo, F. Bai, State-of-health estimation method for fast-charging lithium-ion batteries based on stacking ensemble sparse Gaussian process regression, *Reliab. Eng. Syst. Saf.* 242 (2024) 109787.
- [34] S. Yang, C. Zhang, J. Jiang, W. Zhang, L. Zhang, Y. Wang, Review on state-of-health of lithium-ion batteries: characterizations, estimations and applications, *J. Clean. Prod.* 314 (2021) 128015.
- [35] Y. Li, M. Abdel-Moneim, R. Gopalakrishnan, M. Berecibar, E. Nanini-Maury, N. Omar, et al., A quick on-line state of health estimation method for Li-ion battery with incremental capacity curves processed by Gaussian filter, *J. Power Sources* 373 (2018) 40–53.
- [36] S. Kullback, Leibler RAJAoMS, On information and sufficiency 22 (1) (1951) 79–86.
- [37] B. Fuglede, F. Topse, Jensen-Shannon Divergence and Hubert Space Embedding, 2004.
- [38] D. Anseán, M. Dubarry, A. Devie, B.Y. Liaw, V.M. García, J.C. Viera, et al., Fast charging technique for high power LiFePO4 batteries: a mechanistic analysis of aging, *J. Power Sources* 321 (2016) 201–209.
- [39] X. Huang, Z. Cai, A review of video action recognition based on 3D convolution, *Comput. Electr. Eng.* 108 (2023) 108713.
- [40] Chollet F. Xception: deep learning with depthwise separable convolutions. Conference Xception: Deep Learning with Depthwise Separable Convolutions. p. 1800–1807.
- [41] Wang Q, Wu B, Zhu P, Li P, Hu Q. ECA-net: efficient channel attention for deep convolutional neural networks. Conference ECA-Net: Efficient Channel Attention for Deep Convolutional Neural Networks.
- [42] Sergey I, Christian S. Batch Normalization: Accelerating Deep Network Training by Reducing Internal Covariate Shift. PMLR. p. 448–456.
- [43] Wang CY, Bochkovskiy A, Liao HYMjae-p. YOLOv7: trainable bag-of-freebies sets new state-of-the-art for real-time object detectors. 2022.
- [44] Szegedy C, Vanhoucke V, Ioffe S, Shlens J, Wojna Z. Rethinking the Inception Architecture for Computer Vision. Conference Rethinking the Inception Architecture for Computer Vision. p. 2818–2826.
- [45] Q. Li, Y. Zou, G.H. Long, W. Wu, Ferromagnetic resonance over-voltage identification method based on Gram angle field, *Energy Rep.* 8 (2022) 546–558.
- [46] H. Yuning, C. Chunna, H. Yongping, F.U. Guoqiang, University SLJJoSLU. A Particle Filter Algorithm Based on Markov Transition Nonlinear Systems, 2018.